

A theoretical and experimental study of lens centring errors and their influence on optical image quality

H. H. HOPKINS and H. J. TIZIANI

Physics Department, Imperial College, London

MS. received 15th July 1965

Abstract. Any small decentring of a surface of an optical system may be resolved into an angular tilt of the surface about its intersection with the optical axis and a second-order displacement along the axis. A simple method is described for calculating the lateral shift and coma of the axial image resulting from a surface tilt, and also the contribution of this axial coma to the variance of the wavefront aberration. This leads to a system of tolerances for the tilt and eccentricity of any simple or compound component, and for cementing errors in the latter case. The applications of the resulting formulae are illustrated with examples.

An optical unit has been constructed, with which the tilt error of each surface of a compound system may be measured. The axial coma of a decentred system may be measured using a wavefront-reversing interferometer which is also described.

The decentring errors of a badly mounted microscope objective have been measured, and the axial coma expected from the theory determined interferometrically. Good confirmation of the theory was obtained, and star images further confirm the order of magnitude of the axial coma.

1. Introduction

Optical design has progressed to the point where in many cases the quality of the image is significantly impaired only by production errors, among which centring errors are frequently the important ones.

A number of workers has considered the influence of decentring on the aberrations of optical systems. Maréchal (1950), for example, investigated the effects arising from misalignment of the rear part of a system relative to the front part, the separate parts being assumed to be perfectly centred. Using optical path methods, Maréchal derived the new types of aberration terms which are introduced. Hofmann (1960a, b, 1961, 1962, Hofmann and Klebe 1965), on the other hand, using ray methods, considered the influence on the aberrations of the image of the decentring of a single surface. He also considered the effects of combinations of such tilted surfaces.

In the present work the influence of a single decentred surface on the wave aberration, and thence on the Strehl intensity ratio, is found by a simple application of optical path methods. Suitable combinations of the resulting formulae are then used to specify the possible practical sources of centring error for simple and compound components of a lens system. These errors are:

- (i) A tilt of the optical axis of the component.
- (ii) An eccentricity of the optical axis of the component.
- (iii) Centring errors of cemented surfaces relative to the optical axis of the component.

A system of centring tolerances is formulated on this basis, and it is shown how a simple analysis of the axial coma terms introduced may serve as a useful guide in designing the mount for any system.

A method has also been developed for measuring the tilt errors on individual surfaces of a compound system. This has been used to measure the errors of a badly mounted microscope objective. An interferometer has been designed and the interferograms confirm the amount of axial coma in the objective predicted by the formulae.

2. Influence of a surface centring error on the wave aberration along a ray

If a surface of a lens system undergoes a slight decentring, the emerging optical axis is slightly tilted, and coma appears in the image of the axial object point, which is also laterally displaced in the image plane from its true position. To investigate these effects it suffices to calculate the change in optical path length along a typical ray of the axial pencil.

Figure 1(a) shows how a surface tilt introduces this change in optical path. In the notation of the diagram, the paths $P_2Q_2Q_3Q'$ and P_2GP_3P' are the parts of the new and original ray paths between the surface that has been tilted and the element of wave front,

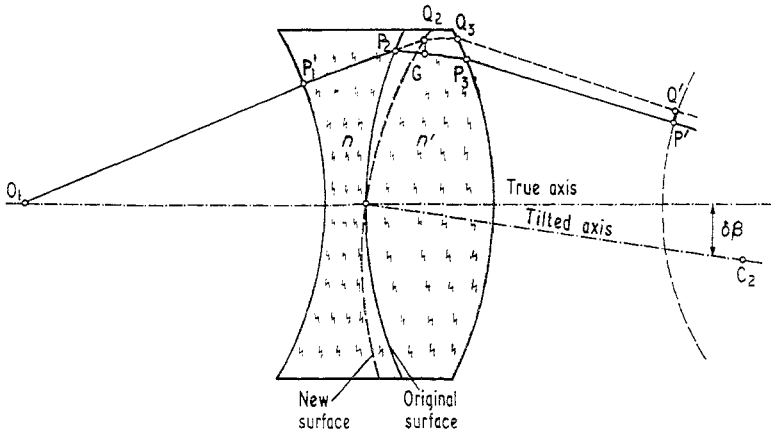


Figure 1(a). Change in optical path due to a surface tilt $\delta\beta$.

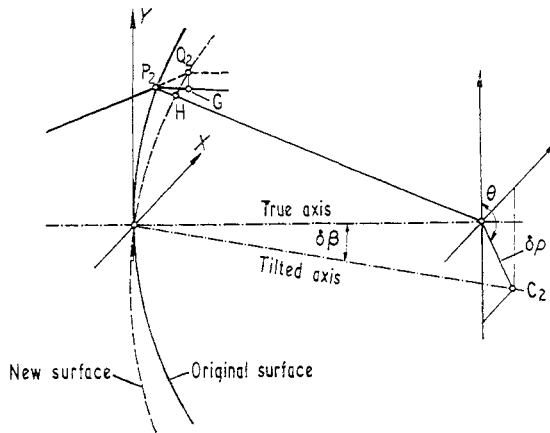


Figure 1(b). Surface tilted in the azimuth θ .

$P'Q'$, in the final image space. The tilted surface is regarded as deriving from the original surface by a 'figuring' $P_2H = f\delta\beta$ measured along the surface normal, where $\delta\beta$ is the angle of tilt and f is the figuring at P_2 produced by unit tilt ($\delta\beta = 1$). The length P_2H is shown in figure 1(b). The point G is the foot of the perpendicular from Q_2 to the original ray. By Fermat's principle, the optical path difference $[Q_2 \dots Q'] - [G \dots P']$, shown in figure 1(a), is of the order of $\delta\beta^2$ and is neglected. To this order of accuracy it then follows that the change in optical path along the given ray, namely

$$\delta P = [O_1P_1P_2Q_2Q_3Q'] - [O_1P_1P_2GP_3P']$$

is given simply by

$$\delta P = [P_2Q_2] - [P_2G]. \tag{1}$$

If now I and I' are the angles of incidence and refraction of the ray at P_2 , that is $I = \angle Q_2P_2H$, $I' = \angle GP_2H$, the path difference (1) may be written

$$\delta P = n \left(\frac{f\delta\beta}{\cos I} \right) - n' \left(\frac{f\delta\beta}{\cos I'} \right) \cos (I - I')$$

which, noting that $n' \sin I' = n \sin I$, easily reduces to

$$\delta P = -f\delta\beta\Delta(n \cos I) \tag{1a}$$

where Δ denotes, as usual, the difference on refraction and n , and n' are refractive indices.

For a tilted surface, the value of f is given by

$$P_2H = f\delta\beta = \{(\delta p \sin \theta) X + (\delta p \cos \theta) Y\} c$$

where θ is the azimuth of the tilt and δp is the distance of the centre of curvature of the tilted surface from the true optical axis. The curvature of the surface is c and (X, Y) are the coordinates of the point of incidence P_2 of the ray at the surface, as shown in figure 1(b). The angle of tilt is given by $\delta\beta = \delta pc$; or using polar coordinates (ρ, ϕ) in place of (X, Y) in this formula and cancelling $\delta\beta$ the above relation leaves

$$f = \rho \cos (\phi - \theta) \tag{2}$$

for the parameter f . This formula also holds for an aspheric surface.

The axis, along which there is no change in optical path, is the reference ray for the axial pencil. Noting that the change in wave aberration is given by

$$\delta W = \delta [\text{reference ray}] - \delta [\text{aperture ray}] \tag{3}$$

where the brackets denote optical path lengths from the object point to the reference sphere in the image space, the formulae (1a) and (2) give

$$\delta W = \rho \cos (\phi - \theta) \Delta(n \cos I) \delta\beta \tag{4}$$

for the change in wave aberration due to decentring, the new aberration being referred to the original reference sphere. The optical axis will be tilted in the same azimuth as the surface tilt, the tilt of the axis being expressed by the paraxial form of (4). In this approximation, $X = hx$ and $Y = hy$, where (x, y) are relative coordinates in the entrance pupil and h is the paraxial ray height at the surface in question. The paraxial form of (4) is now found by substituting $\rho = hr$, where (r, ϕ) are polar coordinates in the entrance pupil corresponding to the relative coordinates (x, y) . This gives

$$\delta W_{11} = hr \cos (\phi - \theta) \Delta(n) \delta\beta \tag{5}$$

where the subscripts are used to indicate that (5) denotes merely a transverse shift of the focal point. Thus the wave aberration along the given ray referred to the laterally displaced axial image point will be given by

$$\delta W = \{\rho\Delta(n \cos I) - hr\Delta(n)\} \delta\beta \cos (\phi - \theta). \tag{6}$$

Both terms on the right hand side of equation (6) are odd functions of the aperture, as is to be expected. Whereas (4) contains a series of terms in odd powers of the aperture including the first, (6) has this latter term removed. Thus the different powers in (6) will be the cube, fifth, etc., representing primary and higher orders respectively of coma.

The formula (6) gives the aberration in the azimuth ϕ produced by a tilt $\delta\beta$ in the azimuth θ . In the analysis given later, however, it proves convenient for the change in aberration due to decentring to be referred to the reference sphere centred on the original image point.† (5) is then not subtracted out from (4). A number of meridian rays from this

† It is, nevertheless, often useful to calculate (6) using $\theta = \phi$ for a number of rays to get a quick order of magnitude value for surface tolerances on decentring.

point is traced through the centred system and, for any surface, the value of ρ is put equal to the incidence height of the ray, Y . The differential coefficient

$$\frac{\partial W}{\partial \beta} = Y\Delta(n \cos I) \quad (7)$$

is then found for the azimuth $\phi = \theta$. It is shown in the next section how these results may then be analysed usefully.

3. Analysis of computed values of axial coma

For an optical system satisfying the sine condition, it may be shown that, for any ray, $x' = x$, $y' = y$, where (x, y) and (x', y') are relative coordinates of the points where this ray cuts the entrance and exit pupil reference spheres respectively. These coordinates are defined as follows. The entrance and exit pupil surfaces are identified with the reference spheres centred on the axial object and image points respectively. Let h and h' be the incidence heights of a paraxial ray at the entrance and exit pupils, and let a finite ray intersect the pupil surfaces at the points (X, Y) and (X', Y') . Then

$$x = \frac{X}{h}, \quad y = \frac{Y}{h}, \quad x' = \frac{X'}{h'}, \quad y' = \frac{Y'}{h'}$$

define the relative coordinates, which have been used in polar form in (5) above. If the paraxial ray is calculated with the same numerical aperture as the full aperture of the system, the circles $x^2 + y^2 = 1$ and $x'^2 + y'^2 = 1$ define the peripheries of the entrance and exit pupils.

The wave aberration of any nominally corrected system may thus be represented by a polynomial using equally (x, y) or (x', y') . Choosing the former, the axial coma terms arising from a tilted surface may be written in the form

$$\delta W(x, y) = \delta W_{31}(x^2 + y^2)y + \delta W_{51}(x^2 + y^2)^2y + \delta W_{71}(x^2 + y^2)^3y + \dots \quad (8)$$

where δW denotes the change in aberration of the ray (x, y) of the axial pencil arising from tilting of a surface. If the surface is assumed to be tilted in the azimuth $\theta = 0$ ($x = 0$) and the aberration is referred to the original reference sphere, the axial aberration along the ray $y = y_j$ resulting from decentring will be of the form

$$\delta W_j = \delta W_{11}y_j + \delta W_{31}y_j^3 + \delta W_{51}y_j^5 + \delta W_{71}y_j^7 + \dots \quad (9)$$

where a transverse shift, denoted by δW_{11} , is included in the polynomial.

The values of δW_j in (9) are referred to the undisplaced axial image point, as in (4) rather than (6). If A rays are chosen such that

$$x_j = 0, \quad y_j = \left(\frac{(A+1) - j}{A} \right)^{1/2} \quad \text{with } j = 1, 2, \dots, A \quad (10)$$

they will be equally spaced in the square of the aperture radius. For any particular value of A the number of orders of coma used in (9) will be $A - 1$ which, with the lateral shift term, give a total of A coefficients. There will be A values of δW_j , one for each of the rays specified in (10), and these will give A equations of the form (9). For any value of A , the values of y_j given by (10) are substituted in (9) and the resulting equations may then be inverted to give:

$$\left. \begin{aligned} \delta W_{11} &= K(1, 1; 1) \delta W_1 + K(1, 1; 2) \delta W_2 + K(1, 1; 3) \delta W_3 + K(1, 1; 4) \delta W_4 \dots \\ \delta W_{31} &= K(3, 1; 1) \delta W_1 + K(3, 1; 2) \delta W_2 + K(3, 1; 3) \delta W_3 + K(3, 1; 4) \delta W_4 \dots \\ \delta W_{51} &= K(5, 1; 1) \delta W_1 + K(5, 1; 2) \delta W_2 + K(5, 1; 3) \delta W_3 + K(5, 1; 4) \delta W_4 \dots \\ \delta W_{71} &= K(7, 1; 1) \delta W_1 + K(7, 1; 2) \delta W_2 + K(7, 1; 3) \delta W_3 + K(7, 1; 4) \delta W_4 \dots \end{aligned} \right\} \quad (11)$$

which express the wave aberration coefficients as linear combinations of the changes in the wave aberrations, δW_j , produced along the rays $j = 1, 2, \dots, A$. The coefficients

Table 1. The coefficients $K(m, n; j)$

$A = 3$

	j		
	1	2	3
$K(1, 1; j)$	1.000 00	-3.674 235	5.196 15
$K(3, 1; j)$	-4.500 00	14.696 94	-12.990 38
$K(5, 1; j)$	4.500 00	-11.022 70	7.794 229

$A = 4$

	j			
	1	2	3	4
$K(1, 1; j)$	-1.000 00	4.618 80	-8.485 28	8.000 00
$K(3, 1; j)$	7.333 33	-32.331 61	53.740 11	-34.666 67
$K(5, 1; j)$	-16.000 00	64.663 23	-90.509 67	48.000 00
$K(7, 1; j)$	10.666 67	-36.950 42	45.254 83	-21.333 33

$A = 5$

	j				
	1	2	3	4	5
$K(1, 1; j)$	1.000 0	-5.590 17	12.909 94	-15.811 39	11.180 34
$K(3, 1; j)$	-10.416 67	56.833 39	-125.872 0	140.984 9	-71.740 51
$K(5, 1; j)$	36.458 33	-190.997 5	395.367 0	-388.696 6	165.375 9
$K(7, 1; j)$	-52.083 33	256.216 1	-484.123 1	428.225 1	-163.046 6
$K(9, 1; j)$	26.041 67	-116.461 9	201.717 9	-164.702 0	58.230 97

A represents the number of rays traced.

$K(m, n; j)$ are functions of y_j only; and so, once A has been chosen, they are independent of the particular optical system studied. Their values have been calculated for the cases $A = 3, 4$ and 5 and are shown in table 1. In the case treated here n is always equal to unity, but this is included for the sake of uniformity with the notation when this technique is used in other problems. Choosing y_j according to (10) leads to well-conditioned equations (9), and thus to accurate numerical values for the coefficients in (11).

The derivatives of the aberration coefficients with respect to the tilt angle $\delta\beta$ of each surface are given from (11) by

$$\frac{\partial W_{m,1}}{\partial \beta} = \sum_{j=1}^A K(m, 1; j) \frac{\partial W_j}{\partial \beta}. \tag{12}$$

The derivatives so obtained indicate the relative sensitivity of the different orders of coma to tilt of the different surfaces of the given system. The term $\partial W_{11}/\partial \beta$ corresponds to lateral image shift.

The formulae (11) give the lateral image shift and the different orders of coma introduced by the tilt of a single surface. If a number of surfaces are decentered in different azimuths, the aberrations of a given order now will be shown to add in a simple manner. Let $\delta\beta_s$ be the tilt of the surface s , in the azimuth θ_s . The total axial coma of a given order $W_{m,1}$ resulting from N decentered surfaces is then simply

$$\delta W = \sum_{s=1}^N (\delta W_{m,1})_s r^m \cos(\phi - \theta_s)$$

which, expanding the cosine, is easily regrouped to give

$$\delta W = \delta \bar{W}_{m,1} r^m \cos(\phi - \bar{\theta}_{m,1}) \tag{13}$$

where

$$\delta \bar{W}_{m,1} = \left[\left\{ \sum_{s=1}^N (\delta W_{m,1})_s \cos \theta_s \right\}^2 + \left\{ \sum_{s=1}^N (\delta W_{m,1})_s \sin \theta_s \right\}^2 \right]^{1/2}$$

is the magnitude of the resultant coma of the given order, which appears in the azimuth

$$\bar{\theta}_{m,1} = \tan^{-1} \left(\frac{\sum_{s=1}^N (\delta W_{m,1})_s \sin \theta_s}{\sum_{s=1}^N (\delta W_{m,1})_s \cos \theta_s} \right).$$

Thus the axial coma terms of a given order produced by a number of surfaces tilted in different azimuths add to give a resultant coma of the same order in a definite azimuth. However, the resultant axial comas of the different orders are, in general, in different azimuths.

There is an important conclusion to be drawn from the above result, namely that the resultant primary term δW_{31} of the axial coma may usually be corrected if it is possible to recentre a suitably selected element. Further, for a combination of surfaces all tilted in the same azimuth, $\theta_{m,1}$ is constant, and so the resultant orders of aberration will all be in the same azimuth. The same comment applies to the lateral image shift produced by tilted surfaces.

An alternative way of representing the resultant of a set of coma terms of given order but in different azimuths is to write

$$\delta W = \sum_{s=1}^N (\delta W_{m,1})_s \cos \theta_s r^m \cos \phi + \sum_{s=1}^N (\delta W_{m,1})_s \sin \theta_s r^m \sin \phi \quad (14)$$

that is

$$\delta W = (\delta W_{m,1})_Y r^m \cos \phi + (\delta W_{m,1})_X r^m \sin \phi$$

where

$$\begin{aligned} (\delta W_{m,1})_Y &= \sum_{s=1}^N (\delta W_{m,1})_s \cos \theta_s \\ (\delta W_{m,1})_X &= \sum_{s=1}^N (\delta W_{m,1})_s \sin \theta_s \end{aligned} \quad (15)$$

are the coefficients of resultant coma terms having symmetry axes in the azimuths $\phi = 0$ and $\frac{1}{2}\pi$ respectively. They may be looked upon as the rectangular components of the resultant coma $\delta \bar{W}_{m,1}$. It is the forms (14) and (15) which are usually employed in practical applications.

4. The specification and sources of centring errors of a lens component

A perfectly centred optical component will have the centres of curvature of the surfaces lying on the same straight line, the optical axis. If the component has one or more cemented surfaces, there may be a cementing error for each cemented surface. Tilt of the cemented surface relative to the optical axis is a measure of this error. The position of any component relative to the true mechanical axis of the system of which it forms part may be specified by: (i) a pure tilt γ of its optical axis about the point of intersection of the optical axis with the air-glass surface located on the shoulder of the mount in an azimuth θ_γ ; (ii) an eccentricity (lateral displacement) ϵ of this point in an azimuth θ_ϵ ; (iii) a cementing error σ in an azimuth θ_σ , specified for each cemented surface relative to the optical axis of the given component.

The optical axis of any simple or compound optical component will normally be defined by the join of the centres of curvature of the outer surfaces. For an exactly concentric configuration of the outer surfaces, where the centres of curvature coincide, the optical axis is no longer defined. In such cases it is possible that an optical axis may be defined by one of the outer surfaces and a cemented surface. For a single concentric meniscus, however, there is no such possibility and the surface tilt errors have to be given separately. When an optical axis is defined by means of one outer surface and a cemented surface the other outer surface will have in general a wedge angle ω , in an azimuth θ_ω , which plays the same role as a cementing error. The reason for grouping the tilt errors in this way is that either of the errors (i) or (ii) above will produce tilts of all the surfaces of the component which lie in the same azimuth and so give coma terms on the different surfaces in

the same azimuth. Any mechanical mounting errors may contribute to one or both of γ and ϵ .

In accordance with (14) and (15), it will be convenient in what follows to express an angular tilt error $\delta\beta$ in the azimuth θ in terms of $\delta\beta_X$ and $\delta\beta_Y$, where

$$\sin \delta\beta_X = \sin \delta\beta \sin \theta \quad \sin \delta\beta_Y = \sin \delta\beta \cos \theta \quad (16)$$

or, for small values of $\delta\beta$,

$$\delta\beta_X = \delta\beta \sin \theta \quad \delta\beta_Y = \delta\beta \cos \theta. \quad (16a)$$

The expressions (16) determine the line joining the centre of curvature C and the intersection of the true axis with the surface. The components (16a) are directly additive for tilt errors on each surface. The axial thickness between the surfaces s and $(s + 1)$ will be denoted by d_s ; and c_s will be used for curvature of the surface s .

(i) Tilt error γ of the optical axis

This case may arise when, for example, the mounting shoulder is tilted as shown in figure 2. If the component has no eccentric error ϵ and no cementing error σ , the individual surface

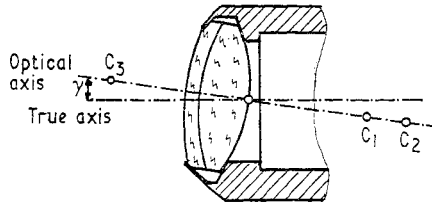


Figure 2. Component showing pure tilt γ of the optical axis.

tilts arising from the tilt error γ of the optical axis, in an azimuth θ_γ , for a cemented doublet component are:

$$\begin{aligned} \delta\beta_{X1} &= [1 - (d_1 + d_2) c_1] \sin \gamma \sin \theta_\gamma & \delta\beta_{Y1} &= [1 - (d_1 + d_2) c_1] \sin \gamma \cos \theta_\gamma \\ \delta\beta_{X2} &= [1 - d_2 c_2] \sin \gamma \sin \theta_\gamma & \delta\beta_{Y2} &= [1 - d_2 c_2] \sin \gamma \cos \theta_\gamma \\ \delta\beta_{X3} &= \sin \gamma \sin \theta_\gamma & \delta\beta_{Y3} &= \sin \gamma \cos \theta_\gamma. \end{aligned} \quad (17)$$

These formulae give the surface tilts corresponding to pure tilt of the optical axis. In practice there will usually be a combination of this with other errors.

(ii) Eccentric error ϵ of the optical axis

This is a lateral displacement ϵ of the optical axis of the component as shown in figure (3). It may arise from eccentricity of the shoulder on which the component is located, or from a

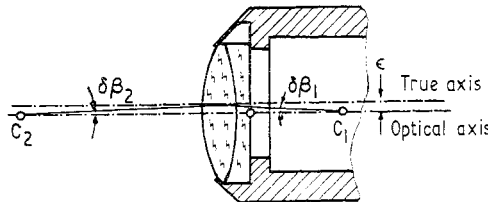


Figure 3. Component with eccentricity ϵ of the optical axis.

lateral displacement of the component in the mount. The contributions of ϵ to the surface errors for a doublet component are:

$$\begin{aligned} \delta\beta_{X1} &= -\epsilon c_1 \sin \theta_e & \delta\beta_{Y1} &= -\epsilon c_1 \cos \theta_e \\ \delta\beta_{X2} &= -\epsilon c_2 \sin \theta_e & \delta\beta_{Y2} &= -\epsilon c_2 \cos \theta_e \\ \delta\beta_{X3} &= -\epsilon c_3 \sin \theta_e & \delta\beta_{Y3} &= -\epsilon c_3 \cos \theta_e. \end{aligned} \quad (18)$$

This eccentric error can, of course, exist together with a tilt of the optical axis, either in the same or in a different azimuth.

(iii) *Cementing error σ of a cemented surface*

The cementing error σ is defined by the tilt of the cemented surface with respect to the optical axis defined by the centres of curvature of the outer surfaces, as illustrated in figure 4.

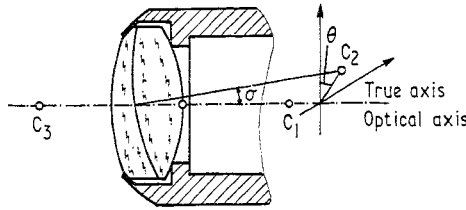


Figure 4. Component with a cementing error σ in the azimuth θ_σ .

The contributions of a cementing error σ to the surface errors for a doublet are:

$$\begin{aligned} \delta\beta_{X_1} &= 0 & \delta\beta_{Y_1} &= 0 \\ \delta\beta_{X_2} &= \sigma \sin \theta_\sigma & \delta\beta_{Y_2} &= \sigma \cos \theta_\sigma \\ \delta\beta_{X_3} &= 0 & \delta\beta_{Y_3} &= 0. \end{aligned} \quad (19)$$

4.1. *Combination of centring errors*

In a practical case the errors (i), (ii) and (iii) may be simultaneously present. For the case of a cemented doublet, the total components of surface tilts will be given by (17), (18) and (19) as

$$\begin{aligned} \delta\beta_{X_1} &= [1 - (d_1 + d_2) c_1] \sin \gamma \sin \theta_\gamma - \epsilon c_1 \sin \theta_e \\ \delta\beta_{Y_1} &= [1 - (d_1 + d_2) c_1] \sin \gamma \cos \theta_\gamma - \epsilon c_1 \cos \theta_e \\ \delta\beta_{X_2} &= [1 - d_2 c_2] \sin \gamma \sin \theta_\gamma - \epsilon c_2 \sin \theta_e + \sigma \sin \theta_\sigma \\ \delta\beta_{Y_2} &= [1 - d_2 c_2] \sin \gamma \cos \theta_\gamma - \epsilon c_2 \cos \theta_e + \sigma \cos \theta_\sigma \\ \delta\beta_{X_3} &= \sin \gamma \sin \theta_\gamma - \epsilon c_3 \sin \theta_e \\ \delta\beta_{Y_3} &= \sin \gamma \cos \theta_\gamma - \epsilon c_3 \cos \theta_e. \end{aligned} \quad (20)$$

If the tilt errors $\delta\beta$ and azimuths θ have been measured for all surfaces of the lens component, the values of $\delta\beta_X$ and $\delta\beta_Y$ may be found from (16) and the measured errors resolved into a tilt γ and eccentricity ϵ of the optical axis and a cementing error σ relative to it. This requires the above equations to be solved for γ , ϵ and σ . Simple elimination gives

$$\begin{aligned} \epsilon \sin \theta_e &= \frac{[1 - (d_1 + d_2) c_1] \delta\beta_{X_3} - \delta\beta_{X_1}}{c_1 - c_3 + (d_1 + d_2) c_1 c_3} \\ \epsilon \cos \theta_e &= \frac{[1 - (d_1 + d_2) c_1] \delta\beta_{Y_3} - \delta\beta_{Y_1}}{c_1 - c_3 + (d_1 + d_2) c_1 c_3} \end{aligned} \quad (21)$$

from which the eccentric error ϵ and its azimuth θ_e are easily found, using

$$\begin{aligned} \epsilon &= \{(\epsilon \sin \theta_e)^2 + (\epsilon \cos \theta_e)^2\}^{1/2} \\ \tan \theta_e &= \frac{[1 - (d_1 + d_2) c_1] \delta\beta_{X_3} - \delta\beta_{X_1}}{[1 - (d_1 + d_2) c_1] \delta\beta_{Y_3} - \delta\beta_{Y_1}}. \end{aligned} \quad (22)$$

Similarly, the components of the cementing error are given by:

$$\begin{aligned} \sigma \sin \theta_\sigma &= \epsilon \sin \theta_e (c_2 - c_3 + d_2 c_2 c_3) + \delta\beta_{X_2} - \delta\beta_{X_3} (1 - d_2 c_2) \\ \sigma \cos \theta_\sigma &= \epsilon \cos \theta_e (c_2 - c_3 + d_2 c_2 c_3) + \delta\beta_{Y_2} - \delta\beta_{Y_3} (1 - d_2 c_2) \end{aligned}$$

from which are found

$$\begin{aligned}\sigma &= \{(\sigma \sin \theta_\sigma)^2 + (\sigma \cos \theta_\sigma)^2\}^{1/2} \\ \tan \theta_\sigma &= \frac{\sigma \sin \theta_\sigma}{\sigma \cos \theta_\sigma}.\end{aligned}\tag{23}$$

Finally, the components of the tilt of the optical axis are obtained from the relations

$$\begin{aligned}\sin \gamma \sin \theta_\gamma &= \delta\beta_{X_3} + \epsilon c_3 \sin \theta_\epsilon \\ \sin \gamma \cos \theta_\gamma &= \delta\beta_{Y_3} + \epsilon c_3 \cos \theta_\epsilon\end{aligned}$$

whence

$$\begin{aligned}\sin \gamma &= \{(\sin \gamma \sin \theta_\gamma)^2 + (\sin \gamma \cos \theta_\gamma)^2\}^{1/2} \\ \tan \theta_\gamma &= \frac{\sin \gamma \sin \theta_\gamma}{\sin \gamma \cos \theta_\gamma}\end{aligned}\tag{24}$$

give the tilt γ and the azimuth θ_γ .

In this manner any errors may be resolved into tilt and eccentricity of the optical axis and one or more cementing errors. It should be re-emphasized that each of the first two of these errors γ and ϵ correspond to tilt errors on all three surfaces in the same azimuth, each of which therefore introduces coma terms in the same azimuth.

The surface derivatives (7) may likewise be combined to express the influence of tilt and eccentricity of any component. A tilt of the optical axis will give, using (17), surface tilts of magnitude

$$\delta\beta_1 = [1 - (d_1 + d_2) c_1] \sin \gamma \quad \delta\beta_2 = [1 - d_2 c_2] \sin \gamma \quad \delta\beta_3 = \sin \gamma \tag{25}$$

so that, when γ is small,

$$\frac{\partial W}{\partial \gamma} = \frac{\partial \beta_1}{\partial \gamma} \frac{\partial W}{\partial \beta_1} + \frac{\partial \beta_2}{\partial \gamma} \frac{\partial W}{\partial \beta_2} + \frac{\partial \beta_3}{\partial \gamma} \frac{\partial W}{\partial \beta_3}$$

giving

$$\frac{\partial W}{\partial \gamma} = [1 - (d_1 + d_2) c_1] \frac{\partial W}{\partial \beta_1} + [1 - d_2 c_2] \frac{\partial W}{\partial \beta_2} + \frac{\partial W}{\partial \beta_3} \tag{26}$$

for the derivative of the aberration along any given ray with respect to tilt of the axis of components. It should be noted that γ may not be small for a near-concentric meniscus element, as is discussed below; (26) is then not applicable. The magnitude of $\partial W/\partial \gamma$ is found using the values of $\partial W/\delta\beta$ calculated for the azimuth $\phi = 0$. Similarly, an eccentric error of the optical axis gives, using (18), surface tilts of magnitude

$$\delta\beta_1 = -c_1\epsilon \quad \delta\beta_2 = -c_2\epsilon \quad \delta\beta_3 = -c_3\epsilon$$

and the derivative of the aberration along a ray with respect to eccentricity is

$$\frac{\partial W}{\partial \epsilon} = - \left(c_1 \frac{\partial W}{\partial \beta_1} + c_2 \frac{\partial W}{\partial \beta_2} + c_3 \frac{\partial W}{\partial \beta_3} \right).\tag{27}$$

By contrast, a cementing error by itself affects only the one surface, so that

$$\frac{\partial W}{\partial \sigma} = \frac{\partial W}{\partial \beta_s} \tag{28}$$

where s is the number denoting the cemented surface.

From (21) it is seen that the analysis used above is no longer applicable when

$$c_1 - c_3 + (d_1 + d_2) c_1 c_3 = 0.\tag{29}$$

The distance between the centres of curvatures is $C_1 C_3 = (d_1 + d_2) + r_3 - r_1$ where r_1 and r_3 are radii of curvature corresponding to c_1 and c_3 . It follows that (29) expresses the condition for a concentric configuration of the outer surfaces 1 and 3 of the component. As already mentioned, if the component is a cemented one, an optical axis may still be

defined by the join of the centres of one cemented surface and one of the outer surfaces. The other outer surface may then have a wedge error with respect to this optical axis of ω in an azimuth θ_ω , which can be treated in the same way as a cementing error. For a single near-concentric meniscus, no optical axis can usefully be defined, and the surface errors must be specified individually.

Practical examples will illustrate the different contributions of the mount itself and of the mounting procedure to tilt γ and eccentricity ϵ of the optical axis of a component. The method enables one to specify tolerances on single and cemented lens components and also tolerances for the mount itself and the mounting procedure.

In figure 5 a cemented component is shown with a surface of finite curvature mounted on a true shoulder. If this surface is a plane the error arising is a pure eccentricity of the optical axis, and is treated as such. In the formulae below this corresponds to the special case when $r_3 = \infty$, giving $\gamma_m = 0$, but $r_3 \sin \gamma_m = \epsilon$. For this reason, when $r_3 = \infty$ tolerances are given for eccentricity only. The centring error shown results from out-of-truth of the counter-cell. In these circumstances the component may take different positions, but with the centre of curvature C_3 always on the true axis. There is thus a tilt and eccentricity of the optical axis in the same azimuth, and this is given by

$$\begin{aligned} \gamma &= \gamma_m & \theta_\gamma &= \theta_m \\ \epsilon &= r_3 \sin \gamma_m & \theta_\epsilon &= \theta_m \end{aligned} \quad (30)$$

where γ_m and θ_m measure the angular error and its azimuth in the mounting procedure. Substitution of these values in (20) gives

$$\begin{aligned} \delta\beta_{X_1} &= \{1 - (d_1 \div d_2 \div r_3) c_1\} \sin \gamma_m \sin \theta_m \\ \delta\beta_{Y_1} &= \{1 - (d_1 \div d_2 \div r_3) c_1\} \sin \gamma_m \cos \theta_m \\ \delta\beta_{X_2} &= \{1 - (d_2 \div r_3) c_2\} \sin \gamma_m \sin \theta_m \\ \delta\beta_{Y_2} &= \{1 - (d_2 \div r_3) c_2\} \sin \gamma_m \cos \theta_m \\ \delta\beta_{X_3} &= 0 \\ \delta\beta_{Y_3} &= 0. \end{aligned}$$

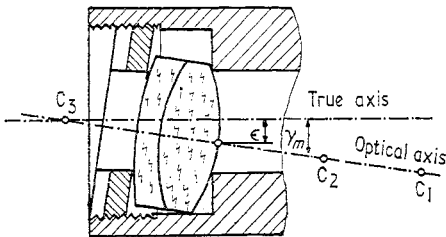


Figure 5. Component with a mounting error γ_m .

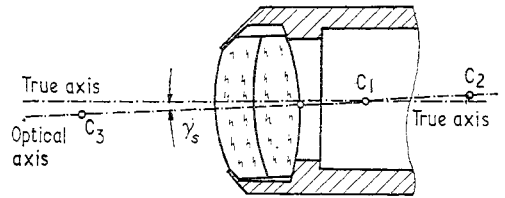


Figure 6. Component with a tilted shoulder but mounted true.

These correspond to surface tilts of magnitude

$$\begin{aligned} \delta\beta_1 &= \{1 - (d_1 \div d_2 \div r_3) c_1\} \sin \gamma_m \\ \delta\beta_2 &= \{1 - (d_2 \div r_2) c_2\} \sin \gamma_m \\ \delta\beta_3 &= 0 \end{aligned}$$

all in the azimuth $\theta = \theta_m$. For this case (26) thus gives, since γ_m will be small,

$$\frac{\partial W}{\partial \gamma_m} = \{1 - (d_1 \div d_2 \div r_3) c_1\} \frac{\partial W}{\partial \beta_1} + \{1 - (d_2 \div r_2) c_2\} \frac{\partial W}{\partial \beta_2} \quad (31)$$

so that, knowing the surface coefficients $\partial W/\partial \beta_1$ and $\partial W/\partial \beta_2$ for any ray, the effect of such a mounting error may easily be found.

Figure 6 shows the effect of an error in the shoulder of the mount, when C_3 can never fall on the true axis; but, in the case shown, the component has been mounted true, that is to say C_1 lies on the true axis. Corresponding to (20) above, there will be a tilt and eccentricity of the optical axis given by

$$\begin{aligned} \gamma &= \gamma_s & \theta_\gamma &= \theta_s \\ \epsilon &= \{r_1 - (d_1 + d_2)\} \sin \gamma_s & \theta_\epsilon &= \theta_s \end{aligned}$$

where γ_s, θ_s are determined by the shoulder error, which locates C_3 . The resulting surface errors are

$$\begin{aligned} \delta\beta_1 &= 0 \\ \delta\beta_2 &= [1 - (r_1 - d_1) c_2] \sin \gamma_s \\ \delta\beta_3 &= [1 - \{r_1 - (d_1 + d_2)\} c_3] \sin \gamma_s \end{aligned}$$

which are all in the azimuth θ_s . If the first surface is a plane, so that $r_1 = \infty$, γ_s tends to zero and $r_1\gamma_s$ is equal to an eccentricity ϵ . In this case, therefore, the error is treated as a pure eccentricity of the optical axis. For such cases tolerances are given for ϵ . The effect of the shoulder error is given, for each ray, by

$$\frac{\partial W}{\partial \gamma_s} = [1 - \{r_1 - d_1\} c_2] \frac{\partial W}{\partial \beta_2} + [1 - \{r_1 - (d_1 + d_2)\} c_3] \frac{\partial W}{\partial \beta_3} \quad (32)$$

assuming that γ_s is small.

In a practical case these errors may be present together; but, being in different azimuths, they have to be toleranced separately. Different designs of mount and mounting procedure may easily be analysed by the method used in relation to the errors shown in figures 5 and 6, namely by expressing each mechanical error in terms of the resulting tilt and eccentricity of the optical axis. For a concentric configuration of the outer surfaces, the optical axis C_1C_3 will be indeterminate; or, as shown in figure 7, it may be perpendicular to the axis of the outer edge of the element. In the case shown in figure 7, C_2C_3 will define an optical axis and the surface 1 then has a wedge error ω . For a single element with near-concentric surfaces the wedge angle imposes a limit on how accurately the two surfaces of the element may be centred. A tolerance has thus to be imposed on the wedge angle of the element as well as on the mount. The same is true for the cemented surfaces of a compound element, for which tolerances have to be imposed on tilt relative to the optical axis defined by the outer surfaces.

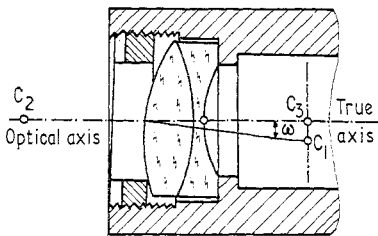


Figure 7. Component with a concentric configuration of the outer surfaces.

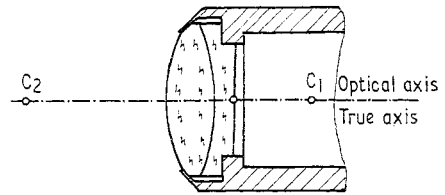


Figure 8. Mounting procedure using shoulder and pilot.

In production practice the design of the mount for a given component will be influenced by the relative sensitivities of the components to tilt and eccentricity errors. These may determine, for example, off which surface the component has to be mounted. In the case where a shoulder and pilot are used, as shown in figure 8, the tilt and eccentricity tolerances specify directly the tolerances on the shoulder and pilot respectively. The tolerance on the tilt of a cemented surface will determine whether a cementing jig is required, or whether sufficient accuracy may result if the elements are merely located relative to their edges.

A further important consideration is the possible advantage that can arise from having

one element whose centring may be adjusted to compensate for the residual errors in other components. The centring tolerances are often so severe that it seems impractical to attempt to mount each surface within the theoretical tolerance. This is particularly so in the case of higher-power microscope objectives.

5. The influence of centring errors on the mean square value of the wave aberration

For each ray of the axial pencil a tilted surface will introduce coma. In order to arrive at a system of tolerances, it is necessary to relate these coma terms to the deterioration in the diffraction image of an axial point source. For this purpose the variance of the wavefront aberration over the pupil area A defined by

$$E = \frac{1}{A} \iint_A W^2 dA - \left(\frac{1}{A} \iint_A W dA \right)^2$$

may be used. Maréchal's treatment of tolerances shows that, for small aberrations, the Strehl intensity ratio is given by the approximate expression:

$$I = \frac{G}{G_0} = \left(1 - \frac{2\pi^2}{\lambda^2} E \right)^2. \quad (33)$$

G and G_0 are the intensities at the best focal point in the presence of the aberration and when $W = 0$, respectively. The even and odd aberrations contribute separately to the variance E , and thus to their effects on the Strehl intensity ratio, provided W is small. For the axial case the only odd aberration terms present are those due to decentring. The variance may thus be written

$$E = (E)_E + (E)_0$$

where $(E)_E$ is the variance arising from the axial spherical aberration terms, and $(E)_0$ that from the axial coma terms.

Let the axial coma of the wave aberration function be written as a polynomial:

$$W_0(r, \phi) = \sum_{n=0}^A W_{2n+1,1} r^{2n+1} \cos(\phi - \theta_n)$$

where $A - 1$ orders of coma are included together with a transverse shift of focus given by the term

$$W_{11} r \cos(\phi - \theta_n).$$

Substituting in the above formula, the value of $(E)_0$ is given by

$$\begin{aligned} (E)_0 &= \frac{1}{\pi} \int_0^1 \int_0^{2\pi} \sum_{n=0}^A \sum_{m=0}^A W_{2n+1,1} W_{2m+1,1} r^{2(n+m+1)+1} \cos(\phi - \theta_n) \cos(\phi - \theta_m) dr d\phi \\ &\quad - \left\{ \frac{1}{\pi} \int_0^1 \int_0^{2\pi} \sum_{n=0}^A W_{2n+1,1} r^{2(n+1)} \cos(\phi - \theta_n) dr d\phi \right\}^2. \end{aligned}$$

The second term vanishes on integrating with respect to ϕ and the remaining integral gives

$$(E)_0 = \sum_{n=0}^A \sum_{m=0}^A W_{2n+1,1} W_{2m+1,1} \frac{\cos(\theta_n - \theta_m)}{2(n+m+2)}. \quad (34)$$

Minimizing the expression (34) with respect to W_{11} determines the best image position in the given focal plane, since W_{11} is a transverse focal shift. Putting the optimum value for W_{11} so obtained in (34) leads to

$$\{(E)_0\}_{W_{11}} = \sum_{n=1}^A \sum_{m=1}^A \frac{nm \delta W_{2n+1,1} \delta W_{2m+1,1}}{2(n+2)(m+2)(n+m+2)} \cos(\theta_n - \theta_m) \quad (35)$$

for the minimum value of $(E)_0$. $\delta W_{2n+1,1}$ and $\delta W_{2m+1,1}$ are here increments in the aberration coefficients resulting from the tilts $\delta\beta$. Substituting for each wave aberration coefficient the linear combination of the wave aberrations as in (11) namely

$$\delta W_{2n+1,1} = \sum_{i=1}^A K_{2n+1,i} \delta W_i$$

now gives

$$\{(E)_0\}_{W_{11}} = \sum_{n=1}^A \sum_{m=1}^A \frac{nm \cos(\theta_n - \theta_m)}{2(n+2)(m+2)(n+m+2)} \sum_{j=1}^A \sum_{i=1}^A K_{2n+1,j} K_{2m+1,i} \delta W_j \delta W_i. \quad (36)$$

(36) shows, as has been mentioned, that different orders of coma can only be easily considered if they are in the same azimuth. It is for this reason that γ and ϵ have been used in §4 above. Thus, when $\theta_m = \theta_n$,

$$\{(E)_0\}_{W_{11}} = \sum_{j=1}^A \sum_{i=1}^A P(i, j) \delta W_j \delta W_i \quad (37)$$

where the coefficients

$$P(i, j) = \sum_{n=1}^A \sum_{m=1}^A \frac{nm K_{2n+1,j} K_{2m+1,i}}{2(n+2)(m+2)(n+m+2)} \quad (38)$$

apply to any system, once A has been decided. It will be seen that

$$P(i, j) = P(j, i)$$

and also that the numerical values of these coefficients depend only on the pupil data for the A rays chosen. δW_j denotes the decentring wave aberration for the ray j and is calculated by ray tracing using equation (7) with $\phi = \theta$. The values of the coefficients $P(i, j)$ have been evaluated for $A = 3, 4$ and 5 and are given in table 2.

Calculation of tolerances for some high power microscope objectives have shown that

Table 2. The coefficients $P(i, j)$ for $\{(E)_0\}_{W_{11}}$

$A = 3$		j		
	1	2	3	
$P(1, j)$	0.028 125	-0.022 964	-0.016 238	
$P(2, j)$	-0.022 964	0.131 250	-0.145 841	
$P(3, j)$	-0.016 238	-0.145 841	0.234 375	

$A = 4$		j			
	1	2	3	4	
$P(1, j)$	0.022 257	-0.005 620 7	-0.007 333 2	-0.024 409 2	
$P(2, j)$	-0.005 620 7	0.082 962 8	-0.106 792	0.018 572 8	
$P(3, j)$	-0.007 333 2	-0.106 792	0.248 254	-0.151 447	
$P(4, j)$	-0.024 409 2	0.018 572 8	-0.151 447	0.230 829	

$A = 5$		j				
	1	2	3	4	5	
$P(1, j)$	0.016 146	0.002 888	-0.015 011	-0.012 254	0.001 444	
$P(2, j)$	0.002 888	0.099 890	-0.117 831	0.065 770	-0.095 154	
$P(3, j)$	-0.015 011	-0.117 831	0.245 417	-0.208 820	0.139 458	
$P(4, j)$	-0.012 254	0.065 770	-0.208 820	0.330 688	-0.210 082	
$P(5, j)$	0.001 444	-0.095 154	0.139 458	-0.210 082	0.242 629	

A represents the number of rays traced.

for individual elements these tolerances are very severe. As mentioned previously, an element giving predominantly primary coma on axis can be intentionally decentred to correct the primary axial coma resulting from residual centring errors in the rest of the system. Having an element which corrects at least the first-order axial coma, the tolerances on higher orders may then be calculated on the assumption that both W_{11} and W_{31} have been given optimum values.

The expression (34) has then to be minimized with respect to both W_{11} and W_{31} , the optimum values for W_{11} and W_{31} being found from the relations

$$\frac{\partial(E)_0}{\partial W_{11}} = 0 \quad \text{and} \quad \frac{\partial(E)_0}{\partial W_{31}} = 0.$$

These values substituted in (34) give the expression

$$\{(E)_0\}_{W_{11}, W_{31}} = \sum_{n=2}^A \sum_{m=2}^A \frac{(mn-m)(mn-n) \cos(\theta_n - \theta_m)}{2(n+m+2)(n+3)(n+2)(m+3)(m+2)} \times \delta W_{2n+1,1} \delta W_{2m+1,1} \quad (39)$$

for the variance of the coma aberrations, when best compensated by an intentionally decentred element. Substituting for the wave aberration coefficients $\delta W_{2n+1,1}$ and $\delta W_{2m+1,1}$ the linear combinations of the wave aberrations δW_j along the traced rays (39) leads to the expression

$$\{(E)_0\}_{W_{11}, W_{31}} = \sum_{j=1}^A \sum_{i=1}^A P(i, j) \delta W_i \delta W_j \quad (40)$$

where

$$P(i, j) = \sum_{n=2}^A \sum_{m=2}^A \frac{(mn-m)(mn-n)}{2(n+m+2)(n+3)(n+2)(m+3)(m+2)} K_{2n+1,j} K_{2m+1,i}. \quad (41)$$

These coefficients are again applicable to any systems, once the value of A has been chosen. Their values for $A = 3, 4$ and 5 are given in table 3.

Table 3. Coefficients $P(i, j)$ for $\{(E)_0\}_{W_{11}, W_{31}}$

$A = 3$

	j		
	1	2	3
$P(1, j)$	0.016 875 0	-0.041 335 2	0.029 228 4
$P(2, j)$	-0.041 335 2	0.101 250 1	-0.071 594 6
$P(3, j)$	0.029 228 4	-0.071 594 6	0.050 625 1

$A = 4$

	j			
	1	2	3	4
$P(1, j)$	0.010 158 8	-0.017 595 4	-0.000 000 1	0.010 158 8
$P(2, j)$	-0.017 595 4	0.071 111 1	-0.099 534 8	0.052 786 2
$P(3, j)$	-0.000 000 1	-0.099 534 8	0.243 809 7	-0.172 399 5
$P(4, j)$	0.010 158 8	0.052 786 2	-0.172 399 5	0.132 063 6

$A = 5$

	j				
	1	2	3	4	5
$P(1, j)$	0.011 226	-0.013 617	0.000 238	-0.013 811	0.021 251
$P(2, j)$	-0.013 617	0.044 535	-0.066 695	0.060 547	-0.028 727
$P(3, j)$	0.000 238	-0.066 695	0.198 191	-0.204 011	0.078 095
$P(4, j)$	-0.013 811	0.060 547	-0.204 011	0.330 196	-0.203 821
$P(5, j)$	0.021 251	-0.028 727	0.078 095	-0.203 821	0.162 915

A is the number of rays traced.

In (37) and (40) δW_i and δW_j are the differentials of the wave aberration for the rays i and j . Denoting either of the left hand sides by $(E)_0$ and putting

$$\delta W_j = \left(\frac{\partial W_j}{\partial p} \right) \delta p$$

where δp is either the angle of tilt of a single surface, or one of the parameters $\gamma, \epsilon, \sigma, \gamma_m, \gamma_s, \omega$ defined previously, gives

$$(E)_{0,\min} = \left\{ \sum_{j=1}^A \sum_{i=1}^A P(i, j) \frac{\partial W_i}{\partial p} \frac{\partial W_j}{\partial p} \right\} \delta p^2. \tag{42}$$

If now, from (33), the permissible value of the contribution of the axial coma to the decrease in the Strehl intensity ratio is decided upon, (42) will give the permissible value of the centring error denoted by p . In this way tolerances for each optical component can be specified for any of the chosen parameters, namely $\gamma, \epsilon, \sigma, \gamma_m, \gamma_s, \omega$. By using the values of $P(i, j)$ given by (38) or (41), these tolerances relate respectively to cases where no controlled decentring of an element is used or one where this is made available.

The surface derivatives $\partial W/\partial \beta$ are first found for the selected set of axial rays. A computer programme is used to trace the rays and to calculate the surface derivatives in the process. To find the relative amount of the different values of axial coma arising from decentring, (12) is used. The surface derivatives are also used in (26), (27), (28), (31) and (32) to obtain the values of $\partial W/\partial p$ for any component, with p equal to $\gamma, \epsilon, \sigma, \gamma_m, \gamma_s$ or ω as the case may demand.

6. The measurement of centring errors

6.1. Measurement of tilt on individual surfaces

The general arrangement of the apparatus used is shown in figure 9. The image reflected from each surface of the optical system under test is used to measure the tilt of the

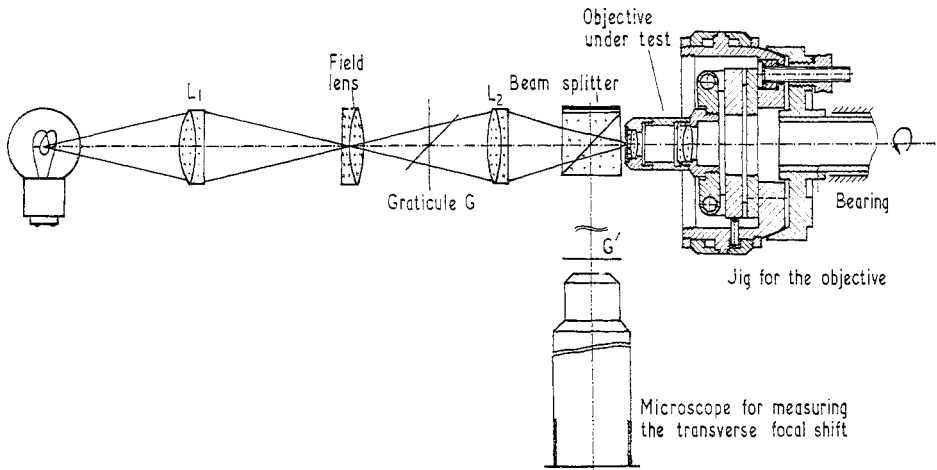


Figure 9. Apparatus for the measurement of eccentric errors.

particular surface relative to the mechanical axis defined by the thread and shoulder of the mount. A graticule G is placed in such a position that the image G' formed by reflection at the selected surface of the objective under test is formed in the object plane of a low power microscope. On rotation of the optical system under test, the image of the graticule describes a circle if the surface is tilted relative to the mechanical axis of rotation. The radius of this circle is measured and from this the angle of tilt of the surface may be deduced.

The lamp filament is imaged by L_1 , at a field lens and then by L_2 at the system under test, which latter therefore also acts as a field lens. Consequently the level of illumination seen at G' is practically independent of the curvatures of the surface of the objective under

test. It is also of importance that the linear displacement of G' is proportional to the tilt of the surface being studied and the sensitivity is almost independent of the radius of the surface.

The graticule consists of a transparent cross made by ruling fine lines on an opaque aluminized disk of glass. A clear graticule with an opaque cross was found to give an image of poor contrast because of stray light. To reduce the stray light the face of the beam splitter remote from the microscope was coated with Canada balsam and lamp black, while the other faces have anti-reflection coatings. The measured reflection coefficients of the surface treated with Canada balsam were measured and found to be less than 0.2% for near normal incidence.

It is necessary to form an image of the lamp between L_1 and L_2 , in order that the position for the graticule giving a focused reflected image at G' be accessible no matter what system is under test. With the arrangement shown, the image of G formed by L_2 may be formed at any position along the axis. For some surfaces, the space between L_1 and the field lens is used for G . The position of the graticule G which gives a final image, after reflection at the selected surface in the object-plane of the microscope objective is found in the paraxial approximation.

The system to be tested is mounted on a jig, which is supported on precision bearings giving an accurately defined mechanical axis. The jig is such that the mechanical axis defined by the bearings may be made to coincide exactly with the optical axis of the objective under test for a perfectly centred objective. This is achieved by accurate adjustment of the objective mount in two perpendicular directions and by a tilt of the jig. The lateral displacement is given by two spirals, in each of which there is a pin which locates the position of the objective mounting. The pins are spring-loaded against the spirals. Accurate adjustment of the jig's angle is obtained by rotation of a spherical surface in a conical seating. These facilities are shown schematically in figure 9.

Adjustment of the optical axis of the system under test relative to the mechanical axis defined by the bearings may be achieved by centring the objective so that the transmitted image of G as observed through the axis of the bearing, does not move when the spindle rotates.

For each surface, in turn, of the system under test, the position of the graticule G has to be determined such that the light reflected at the given surface forms an image of G at G' . A paraxial ray is thus traced backwards from G' , through the system to a surface S ; then, after reflection at this surface, the trace is continued in the reverse direction out to the image space of the lens L_2 . The light traverses this path in the opposite direction, and the lateral displacement of the image G' will be the superposed effects of the decentring of all the surfaces 1, 2, . . . S . The contribution of each surface to this displacement of G' may be expressed by the transverse focal shift term given in (5). For the marginal paraxial ray in the meridian section $r = 1$ in (5). The resultant transverse shift is given, using (13) with $m = 1$, by

$$\begin{aligned} \delta \bar{W}_{11} \cos(\phi - \bar{\theta}) = & \sum_{s=1}^{S-1} h_s(n' - n)_s \cos(\phi - \theta_s) \delta\beta_s \\ & + h_s(-n_s - n_s) \cos(\phi - \theta_s) \delta\beta_s \\ & + \sum_{s=S-1}^1 h_s^*(n - n')_s \cos(\phi - \theta_s) \delta\beta_s \end{aligned}$$

where $\delta \bar{W}_{11}$ is the magnitude of the transverse focal shift and $\bar{\theta}$ its azimuth, n_s and n'_s are refractive indices of the object and image space for the surface s for light travelling from left to right through the system. h_s, h_s^* are the incident heights of the paraxial ray at surface s for the left-to-right and right-to-left passage of the light respectively. Collecting terms, the above expression gives

$$\begin{aligned} \delta \bar{W}_{11} \cos(\phi - \bar{\theta}) = & \sum_{s=1}^{S-1} (h_s - h_s^*)(n' - n)_s \cos(\phi - \theta_s) \delta\beta_s \\ & - 2h_s n_s \cos(\phi - \theta_s) \delta\beta_s. \quad (43) \end{aligned}$$

In practice the angle $\bar{\theta}$ is measured by setting the angle of the system under test such that the image G' is displaced to the right in the horizontal direction as seen by a graticule cross-line. The value of $\delta\bar{W}_{11}$ is found from the relation

$$\delta\bar{W}_{11} = n'u' \delta\eta' \tag{44}$$

where $\delta\eta'$ is the radius of the circle described by G' on rotation of the system under test, u' is the paraxial angle in the space of G' used for the traced paraxial rays. The refractive index n' of this space will normally be equal to unity.

Expanding the cosines in (43) gives for the rectangular components of the two sides

$$\begin{aligned} (\delta\bar{W}_{11})_Y &= \delta\bar{W}_{11} \cos \bar{\theta} = \sum_{s=1}^{S-1} (h_s - h_s^*)(n' - n)_s \cos \theta_s \delta\beta_s - 2h_s n_s \cos \theta_s \delta\beta_s \\ (\delta\bar{W}_{11})_X &= \delta\bar{W}_{11} \sin \bar{\theta} = \sum_{s=1}^{S-1} (h_s - h_s^*)(n' - n)_s \sin \theta_s \delta\beta_s - 2h_s n_s \sin \theta_s \delta\beta_s \end{aligned}$$

from which

$$\begin{aligned} (\delta\beta_Y)_S &= \delta\beta_S \cos \theta_S = \frac{1}{2h_S n_S} \left\{ \sum_{s=1}^{S-1} (h_s - h_s^*)(n' - n)_s \cos \theta_s \delta\beta_s - \delta\bar{W}_{11} \cos \bar{\theta} \right\} \\ (\delta\beta_X)_S &= \delta\beta_S \sin \theta_S = \frac{1}{2h_S n_S} \left\{ \sum_{s=1}^{S-1} (h_s - h_s^*)(n' - n)_s \sin \theta_s \delta\beta_s - \delta\bar{W}_{11} \sin \bar{\theta} \right\}. \end{aligned} \tag{45}$$

Thus, knowing the values of $\cos \theta_s \delta\beta_s$ and $\sin \theta_s \delta\beta_s$ for $s = 1, 2, \dots, S - 1$, the values of $\delta\beta_S$ and θ_S may be found. The values of $\delta\beta$ and θ are thus found for the surfaces 1, 2 . . . in turn.

If the system under test comprises a compact set of surfaces, the values of h_S will be not very dissimilar at the different surfaces. In this case, a given value of $\delta\eta'$ will correspond to approximately the same value of $\delta\beta$ for any surface. If the system consists of widely separated surfaces, it may happen that the point conjugate to G' falls at or near a surface to be tested. In this case h_S is zero, or small, and an auxiliary lens has to be placed after the beam splitter to image G at -1 magnification. The paraxial ray from G' has then to be traced through this lens also, when h_S will no longer be zero. The case $h_S = 0$ means, geometrically, that the surface being studied acts as a field element and clearly then gives a zero contribution to $\delta\eta'$.

In practice the system to be tested may be well centred in itself, but there may be eccentricity or tilt between its optical axis and the axis defined by the locating thread and shoulder or other mounting location. It then becomes necessary to determine the mean axis of the system and to refer the individual surface errors $(\delta\beta, \theta)$ to the axis so found.

Suppose, for example, the reference axis to be rotated through an angle $\bar{\gamma}$ in an azimuth $\bar{\theta}_\gamma$ about the pole of the first surface of the system, and further that the axis is displaced eccentrically by an amount $\bar{\epsilon}$ in an azimuth $\bar{\theta}_\epsilon$. Referred to this new axis, the rectangular components $\delta\beta_X$ and $\delta\beta_Y$ as calculated using (45) become

$$\begin{aligned} (\delta\tilde{\beta}_X)_s &= \delta\beta_s \sin \theta_s - \bar{\gamma} \sin \bar{\theta}_\gamma \{c_s(d_1 + d_2 + \dots + d_{s-1}) + 1\} - \bar{\epsilon} \sin \bar{\theta}_\epsilon c_s \\ (\delta\tilde{\beta}_Y)_s &= \delta\beta_s \cos \theta_s - \bar{\gamma} \cos \bar{\theta}_\gamma \{c_s(d_1 + d_2 + \dots + d_{s-1}) + 1\} - \bar{\epsilon} \cos \bar{\theta}_\epsilon c_s \end{aligned} \tag{46}$$

or, putting

$$\begin{aligned} \bar{\gamma}_X &= \bar{\gamma} \sin \bar{\theta}_\gamma & \bar{\gamma}_Y &= \bar{\gamma} \cos \bar{\theta}_\gamma \\ \bar{\epsilon}_X &= \bar{\epsilon} \sin \bar{\theta}_\epsilon & \bar{\epsilon}_Y &= \bar{\epsilon} \cos \bar{\theta}_\epsilon \end{aligned} \tag{47}$$

and using rectangular components throughout in (46), these latter become

$$\begin{aligned} (\delta\tilde{\beta}_X)_s &= (\delta\beta_X)_s - \bar{\gamma}_X \{c_s(d_1 + d_2 \dots + d_{s-1}) + 1\} - \bar{\epsilon}_X c_s \\ (\delta\tilde{\beta}_Y)_s &= (\delta\beta_Y)_s - \bar{\gamma}_Y \{c_s(d_1 + d_2 \dots + d_{s-1}) + 1\} - \bar{\epsilon}_Y c_s. \end{aligned} \tag{48}$$

The mean axis will be defined by the values of $\bar{\gamma}_X, \bar{\gamma}_Y, \bar{\epsilon}_X$ and $\bar{\epsilon}_Y$ which minimize the sums of the squares of $(\delta\tilde{\beta}_X)_s$ and $(\delta\tilde{\beta}_Y)_s$. Thus write

$$M = \sum_{s=1}^S (\delta\tilde{\beta}_X)_s^2 + \sum_{s=1}^S (\delta\tilde{\beta}_Y)_s^2 = \sum_{s=1}^S (\delta\beta)_s^2 \tag{49}$$

and then

$$M = \sum_{s=1}^S \{(\delta\beta_X)_s - \bar{\gamma}_X[c_s(d_1 + d_2 + \dots + d_{s-1}) + 1] - \bar{\epsilon}_X c_s\}^2 + \sum_{s=1}^S \{(\delta\beta_Y)_s - \bar{\gamma}_Y[c_s(d_1 + d_2 + \dots + d_{s-1}) + 1] - \bar{\epsilon}_Y c_s\}^2.$$

The conditions for M to be a minimum are

$$\frac{\partial M}{\partial \bar{\gamma}_X} = \frac{\partial M}{\partial \bar{\gamma}_Y} = \frac{\partial M}{\partial \bar{\epsilon}_X} = \frac{\partial M}{\partial \bar{\epsilon}_Y} = 0 \quad (50)$$

and (49) then gives the four equations

$$\begin{aligned} \bar{\gamma}_X \left\{ \sum_{s=1}^S A_s^2 \right\} + \bar{\epsilon}_X \left\{ \sum_{s=1}^S c_s A_s \right\} - \left\{ \sum_{s=1}^S A_s (\delta\beta_X)_s \right\} &= 0 \\ \bar{\gamma}_Y \left\{ \sum_{s=1}^S A_s^2 \right\} + \bar{\epsilon}_Y \left\{ \sum_{s=1}^S c_s A_s \right\} - \left\{ \sum_{s=1}^S A_s (\delta\beta_Y)_s \right\} &= 0 \\ \bar{\gamma}_X \left\{ \sum_{s=1}^S c_s A_s \right\} + \bar{\epsilon}_X \left\{ \sum_{s=1}^S c_s^2 \right\} - \left\{ \sum_{s=1}^S c_s (\delta\beta_X)_s \right\} &= 0 \\ \bar{\gamma}_Y \left\{ \sum_{s=1}^S c_s A_s \right\} + \bar{\epsilon}_Y \left\{ \sum_{s=1}^S c_s^2 \right\} - \left\{ \sum_{s=1}^S c_s (\delta\beta_Y)_s \right\} &= 0 \end{aligned} \quad (51)$$

where

$$A_s = c_s(d_1 + d_2 + \dots + d_{s-1}) + 1 \quad (52)$$

which are easily solved for $\bar{\epsilon}_X$, $\bar{\epsilon}_Y$, $\bar{\gamma}_X$ and $\bar{\gamma}_Y$. The relations (48) then give

$$(\delta\tilde{\beta}_X) = \delta\tilde{\beta} \sin \tilde{\theta} \quad (\delta\tilde{\beta}_Y) = \delta\tilde{\beta} \cos \tilde{\theta} \quad (53)$$

from which the tilt $\delta\tilde{\beta}$ and azimuth $\tilde{\theta}$ of each surface relative to the best mean optical axis are found.

For a photographic objective an eccentricity $\bar{\epsilon}$ of the mean optical axis relative to the mechanical axis of the mount will normally be of no consequence. On the other hand, a non-zero value for $\bar{\gamma}$ will mean that the plane in which the image is formed is not exactly perpendicular to the axis of the mount. For a microscope objective both these eccentricity and tilt errors will usually need to be extremely small.

6.1. Interferometric measurement of axial coma in the presence of spherical aberration

To study the total effect of centring errors in an optical system in the presence of spherical aberration, an interferometer has been devised. The asymmetry, which distinguishes the

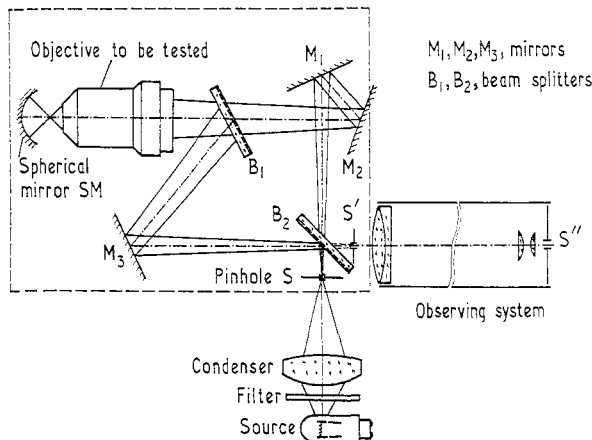


Figure 10. Interferometer for the measurement of axial coma.

coma of the axial image due to centring errors from spherical aberration, can be observed by eliminating effects depending on those aberrations which depend on an even power of the aperture. Figure 10 shows the principle of an interferometer used for this purpose. In passing from S, the wave-front following the path $B_2M_3B_1$ is reversed relative to that following the path $B_2M_1M_2B_1$ because of the additional reflection. Both parts of the wavefront go along similar paths through the system to be tested and are reflected back from a spherical mirror SM. A second reversal of one of the wavefronts relative to the other brings the two previously reversed parts into coincidence. Because of the relative reversal of the two waves only the asymmetrical part of the aberration of the optical system under test is detected. These asymmetrical variations in optical paths are due to axial coma resulting from decentring of the optical elements. The optical path differences as seen in the interferogram are doubled due to relative reversal of the wavefronts and, each wave front being reflected back along a similar path through the optical system under test, four times the asymmetric contribution to the aberrations is shown by the fringe pattern.†

Any asymmetry resulting from tilt of the spherical mirror SM can be eliminated by observing the interference pattern in the two azimuths 0 and π , or in $\frac{1}{4}\pi$ and $\frac{3}{4}\pi$, respectively. The system is auto-collimating and self-compensating, giving a stable fringe pattern. The distance from the pinhole to the objective in this particular arrangement is 160 mm, so that a microscope objective is tested at the correct tube length.

To analyse the interferogram the positions of the fringes along a horizontal diameter are measured and fitted to a wave aberration polynomial in odd powers of the fractional aperture radius r . Thus, where three fringe maxima or minima are present one writes

$$\delta W(r) = \delta W_{11}r + \delta W_{31}r^3 + \delta W_{51}r^5$$

and the coefficients are found by solving three equations of this kind.

7. Practical applications

7.1. Calculated tolerances for microscope objectives

As examples to illustrate the use of the methods described earlier the errors introduced by decentring have been calculated for a $\times 10$ Listertype microscope objective, numerical aperture = 0.28, and also for a $\times 100$ oil immersion, numerical aperture = 1.37. For the $\times 10$ objective three axial rays were used, i.e. $A = 3$, corresponding to two orders of axial coma. For the high power objective five rays were traced, corresponding to $A = 5$ and four orders of coma.

For the $\times 10$ objective the derivatives of the aberration coefficients with respect to surface tilts have been calculated using (12). The results are shown in the first columns of table 4, the units being $\mu\text{m rad}^{-1}$. The coefficient $\partial W_{11}/\partial\beta$ gives the lateral displacement of the image, expressed as a wavefront tilt at the exit pupil. The surface derivatives of the aberration coefficients have also been combined, as in (26) and (27), to show the influence of tilt and eccentricity of the optical axis of each component as a whole. The former are again expressed in $\mu\text{m rad}^{-1}$, and the latter are given in $\mu\text{m mm}^{-1}$. It will be seen that, for either component, an eccentricity of 0.1 mm gives a total coma equal to 0.46 μm . For tilts equal to 0.001 rad (3 minutes of arc) the corresponding aberrations are 0.02 μm and 0.10 μm for the first and second components respectively. These values of axial coma refer to the total aberration along the marginal ray. In fact these comprise different proportions of primary and secondary coma in the different cases.

Tolerances, employing the criterion

$$\{(E)_0\}_{W_{11}} \leq \frac{\lambda^2}{180} \tag{54}$$

corresponding to a 20% reduction in Strehl intensity ratio have been calculated for tilt γ ,

† This method of wavefront reversal was used by Gates (1955), but employing a different optical arrangement.

Table 4. Differential coefficients of the surfaces and components of the $\times 10$ microscope objective

Surface	$\partial W_{11}/\partial\beta$	$\partial W_{31}/\partial\beta$	$\partial W_{51}/\partial\beta$	$\partial W_{11}/\partial\gamma$	$\partial W_{31}/\partial\gamma$	$\partial W_{51}/\partial\gamma$	$\partial W_{11}/\partial\epsilon$	$\partial W_{31}/\partial\epsilon$	$\partial W_{51}/\partial\epsilon$
<i>s</i>									
1	+1175	+75.53	+5.92	—	—	—	—	—	—
2	-225	-36.69	-14.15	-217.4	+19.00	+2.975	-158.9	+0.8224	+3.74
3	-1217	-19.79	+2.15	—	—	—	—	—	—
4	+2600	+63.10	+26.84	—	—	—	—	—	—
5	-456	-51.57	-24.60	-88.0	-87.398	-16.325	-145.6	-4.392	+0.158
6	-2325	-109.5	-23.6	—	—	—	—	—	—

$\partial W/\partial\beta$, $\partial W/\partial\gamma$ in $\mu\text{m rad}^{-1}$, $\partial W/\partial\epsilon$ in $\mu\text{m mm}^{-1}$.

eccentricity ϵ , cementing error σ and mounting error γ_m . The results are shown in table 5, being expressed in terms of radians and millimetres in the different cases. In practice more severe tolerance would be applied and to find these it has only to be noted that $\{(E)_0\}_{W_{11}}$ is proportional to the square of the centring error. Thus, if the value of $\{(E)_0\}_{W_{11}}$ in (54) is made four times smaller, the tolerances in table 5 have to be halved.

Table 5. Calculated tolerances of the single surfaces and components of a $\times 10$ microscope objective for $\{(E)_0\}_{W_{11}}$

Surface	Surface tolerances	Tolerance	Tolerance	Tolerance	Tolerance
<i>s</i>	$\delta\beta$ (rad)	γ (rad)	γ_m (rad)	ϵ (mm)	σ (rad)
1	0.004 283	—	—	—	—
2	0.006 423	0.015 30	0.030 0	0.064	0.006 42
3	0.021 409	—	—	—	—
4	0.003 616	—	—	—	—
5	0.004 248	0.003 23	0.006 42	0.082	0.004 25
6	0.002 50	—	—	—	—

Table 6. Calculated tolerances of single surfaces and components for a high power objective and $\{(E)_0\}_{W_{11}}$

Surface	Surface tolerances	γ (rad)	γ_m (rad)	γ_s (rad)	ϵ (μm)	σ (rad)
<i>s</i>	(rad)					
1	0.095 53	—	—	—	—	—
2	0.013 05	0.013 53	0.095 53	($r_1 = \infty$)	11.3	—
3	0.001 122	—	—	—	—	—
4	0.002 156	0.001 980	0.001 264	0.000 461	8.23	—
5	0.002 737	—	—	—	—	—
6	0.016 28	—	—	—	—	0.016 28
7	0.002 709	—	—	—	—	0.002 709
8	0.003 950	0.082 51	0.003 761	0.000 972	20.2	—
9	0.004 369	—	—	—	—	—
10	0.002 652	—	—	—	—	0.002 652
11	0.005 520	0.006 220	0.001 347	0.000 369	14.0	—

The high power objective had the conventional construction, namely an Amici hemispherical front lens followed successively by a meniscus element, a cemented triplet and finally a cemented doublet. Table 6 shows the tolerances on tilt error for each surface singly and then the tolerances on γ , γ_m , γ_s and ϵ respectively. The cementing tolerances σ_6 , σ_7 and σ_{10} are simply the surface tolerances for $s = 6, 7$ and 10 respectively. The tolerances shown are based on a permissible reduction of 10% in the Strehl intensity ratio, and the variance used is $\{(E)_0\}_{W_{11}}$ that minimized with respect to W_{11} .

Table 7. Surface errors referred to the mechanical axis and the aberrations introduced

Surface	Transverse focal shift		$\delta\beta_x$ (rad)	$\delta\beta_y$ (rad)	$(\delta W_{11})_X$ (μm)	$(\delta W_{11})_Y$ (μm)	$(\delta W_{31})_X$ (μm)	$(\delta W_{31})_Y$ (μm)	$(\delta W_{51})_X$ (μm)	$(\delta W_{51})_Y$ (μm)
	$\delta\eta'$ (mm)	θ								
1	—	—	—	—	—	—	—	—	—	—
2	0.21	90°	-0.3583×10^{-3}	0	+0.0808	—	+0.01314	—	+0.00507	—
3	—	—	—	—	—	—	—	—	—	—
4	0.33	227°	$+7.594 \times 10^{-3}$	-6.728×10^{-3}	-19.7381	-17.4872	+0.47919	-0.42454	+0.20378	-0.18055
5	0.705	325°	$+14.8306 \times 10^{-3}$	$+16.4939 \times 10^{-3}$	-6.7637	-7.5222	-0.76474	-0.85051	-0.36489	-0.40582
6	0.48	10°	-3.6642×10^{-3}	-8.6580×10^{-3}	-18.5178	+20.1264	+0.40123	+0.94805	+0.08648	+0.20433
Total					21.5730	-4.8830	+0.12882	-0.32700	-0.06956	-0.38204

For the high power objective the centring tolerances are given for each surface separately; they are also expressed in terms of γ , γ_m , γ_s , ϵ and σ and are given in radians for angles and micrometres for ϵ . The different tolerances are appropriate to different methods of mounting. The results are shown in table 6. For the front hemisphere the front surface is plane so that no tolerance is given for γ_s ; any error amounts, as has been mentioned earlier, to an eccentricity. These tolerances are based on a 10% reduction in the Strehl intensity ratio, assuming minimization with respect to W_{11} .

7.2. Measurement of surface tilt errors

Centring errors were deliberately introduced in the 16 mm microscope objective used for the calculations in §7.1 above. The cement was softened in the second doublet component, and the lenses displaced. The rear part of the mount was remade to be eccentric and tilted relative to the front half of the system. The objective was then mounted on the adjustable jig described earlier and centred to give no tilt or eccentricity for the front doublet components. The tilt errors on each surface were then measured and analysed as described in §6.1 above.

The measured displacements $\delta\eta'$ in the image plane G' are given in table 7, together with the analysis of these errors into rectangular components of surface tilt, $\delta\beta_X$ and $\delta\beta_Y$, and also the rectangular components $(\delta W_{11})_X$ and $(\delta W_{11})_Y$ of the coma introduced. The resultant components of primary and secondary axial coma are given in the last line of the table. The value of total axial coma at $r = 1$ is 1.30λ in the azimuth $\phi = 355^\circ$.

The mean optical axis was also determined, and this gave the values

$$\begin{aligned}\bar{\gamma} &= 0.0056 \text{ rad} & \bar{\theta}_\gamma &= 53^\circ \\ \bar{\epsilon} &= 0.0158 \text{ mm} & \bar{\theta}_\epsilon &= 358^\circ\end{aligned}$$

and the coma given by the tilts referred to the mean axis was calculated. This gave a value of 1.27λ for $r = 1$, serving as a useful check on the previous value of 1.30λ .

The axial coma of this decentred objective was then determined by means of the wave-front reversing interferometer described in §6.2. The fringe pattern is shown in figure 11(a) (plate)†. This fringe pattern was used to determine the coefficient in the polynomial

$$\delta W(r) = \delta W_{11}r + \delta W_{31}r^3 + \delta W_{51}r^5$$

and gave the values $\delta W_{31} = -0.70\lambda$, $\delta W_{51} = -0.44\lambda$. The coefficient includes a tilt of the spherical mirror and is of no interest. For $r = 1$ these give a total axial coma equal to 1.14λ , which has to be compared with a value of 1.30λ calculated from the measured tilt of the surface. This is satisfactory agreement in view of the possible sources of error.

Figure 11(b) (plate) shows the star image produced by this objective; the appearance is closely consistent with the star pattern for primary coma of the order of 1λ (Cagnet *et al.* 1962).

References

- CAGNET, M., FRANÇON, M., and THRIERR, J. C., 1962, *Atlas of Optical Phenomena* (Berlin: Springer-Verlag) p. 25.
 GATES, V. W., 1955, *Proc. Phys. Soc. B*, **68**, 1065–72.
 HOFMANN, C., 1960a, *Optik, Stuttg.*, **17**, 465–84.
 ——— 1960b, *Jenaer Jb.*, II, **9**, 341–63.
 ——— 1961, *Jenaer Jb.*, I, **10**, 35–65.
 ——— 1962, *Optik, Stuttg.*, **19**, 41–55.
 HOFMANN, C., and KLEBE, J., 1965, *Optik, Stuttg.*, **22**, 95–122.
 MARÉCHAL, A., 1950, *Revue d'Opt. Théor. Instrum.*, **29**, 1–24.

† Plates at end of issue.

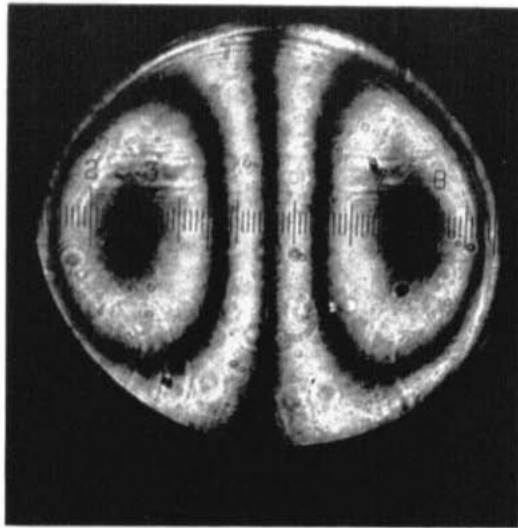


Figure 11(a). Interferogram showing axial coma of a decentered $\times 10$ microscope objective.

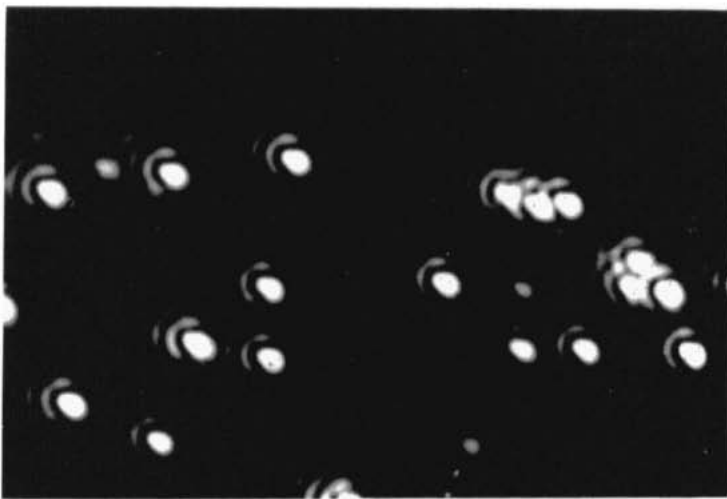


Figure 11(b). Star image of a decentered $\times 10$ microscope objective.